ACS APPLIED MATERIALS & INTERFACES

Research Article

www.acsami.org

Single Domain m-Plane ZnO Grown on m-Plane Sapphire by Radio Frequency Magnetron Sputtering

B. H. Lin,[†,‡] W.-R. Liu,[‡] C. Y. Lin,[†,§] S. T. Hsu,[†] S. Yang,[†] C. C. Kuo,[†] C.-H. Hsu,*[,‡,†] W. F. Hsieh,*[,†] F. S.-S. Chien,[§] and C. S. Chang[†]

[†]Department of Photonics and Institute of Electro-Optical Engineering, National Chiao Tung University, Hsinchu 30010, Taiwan

[‡]Division of Scientific Research, National Synchrotron Radiation Research Center, Hsinchu 30076, Taiwan

[§]Department of Physics, Tunghai University, Taichung 40704, Taiwan

ABSTRACT: High-quality m-plane orientated ZnO films have been successfully grown on m-plane sapphire by using radio frequency magnetron sputtering deposition. The introduction of a nanometer-thick, low-temperature-grown ZnO buffer layer effectively eliminates inclusions of other undesirable orientations. The structure characteristics of the ZnO epi-layers were thoroughly studied by synchrotron X-ray scattering and transmission electron microscopy (TEM). The in-plane epitaxial relationship between ZnO and sapphire follows $(0002)_{ZnO}$ ∥ $(11\bar{2}0)_{sapphire}$ and $(11\bar{2}0)_{ZnO}$ ∥ $(0006)_{sapphire}$ and the ZnO/sapphire interface structure can be described by the domain matching epitaxy along the $[11\bar{2}0]_{ZnO}$ direction. The vibrational properties of the films were investigated by polarization dependent micro-Raman spectroscopy. Both XRD and micro-Raman results reveal that the obtained m-ZnO layers are under an anisotropic biaxial strain but still retains a hexagonal lattice.

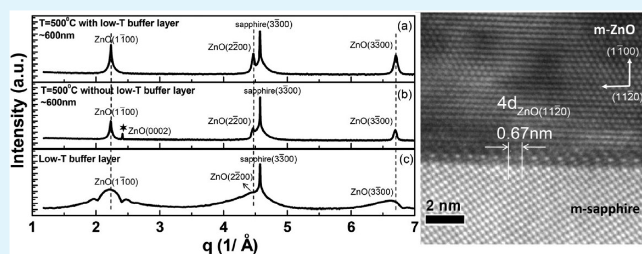

KEYWORDS: *non-polar ZnO, RF-magnetron sputtering, strain, structural defects*

INTRODUCTION

Wurtzite GaN and ZnO are the most promising compound semiconductors for solid-state light-emitting devices. Because of the presence of spontaneous and piezoelectric polarizations along the polar direction, which coincides with the *c*-axis of wurtzite structure, ZnO-based quantum well (QW) structure with c-plane orientation suffers quantum confined Stark effect (QCSE), which reduces the exciton binding energies and limits the optical performance.[1,2] Epitaxial growth of ZnO films with nonpolar orientations, such as $(1\bar{1}00)$ m-plane and $(11\bar{2}0)$ a-plane orientations, provides a solution to avoid this problem. However, the growth of high-quality nonpolar ZnO-based thin films is still far from being mature. The existence of a large density of defects hampers its commercial applications. In the case of m-plane oriented ZnO films, domains of other orientations such as (0002),[3] $(10\bar{1}3)$,[4,5] and $(11\bar{2}2)$[6] often coexist with the m-plane matrix and are detrimental to the electrical and optical performance of the deposited layers. Basal plane stacking faults (BSF) of large density, typically $\geq 1 \times 10^6$ cm^{-1}, are another major structural defects, which act as nonradiative recombination centers and are responsible for poor internal quantum efficiency (IQE).[7] The growth of high-quality ZnO films with pure m-plane orientation remains a subject of great importance and challenge. Epitaxial growth of m-plane ZnO has be achieved on various substrates, such as m-plane sapphire,[8−10] γ-$LiAlO_2$ (100),[11] $LaAlO_3$(112),[12] and $ZnWO_4$ (010).[13] Among them, m-plane sapphire is commercially available and the most common one. We thus adopted m-plane sapphire as the substrate for this study.

Radio frequency (RF) sputtering deposition is a popular film growth technique and has been widely employed in industrial thin film fabrication processes. It has several advantages, such as low cost, large-area deposition, scalability, and high deposition rate. Although the growth of m-plane ZnO has been achieved by using metal organic vapor phase epitaxy,[14] molecular beam epitaxy,[15] and pulsed laser deposition (PLD),[12] no work, to the best of our knowledge, by using radio frequency (RF) magnetron sputtering has been reported so far. In this article, we report the growth of single orientation epitaxial m-plane ZnO films on m-plane sapphire substrates buffered with a layer of low-temperature grown ZnO (LT-ZnO). The structural properties of the m-ZnO/m-sapphire heteroepitaxial system were thoroughly examined by X-ray diffraction (XRD), and transmission electron microscopy (TEM). Vibrational characteristics of the ZnO films were examined by polarized micro-Raman spectra.

EXPERIMENTAL SECTION

ZnO was grown on $(1\bar{1}00)$ m-plane sapphire 10 × 10 mm^2 in size by sputtering a 2" high purity ZnO target (99.995%) using a RF magnetron sputtering system. The chamber was pumped down to a

Received: July 9, 2012
Accepted: September 18, 2012
Published: September 18, 2012

 © 2012 American Chemical Society

base pressure of 1.2×10^{-8} Torr before introducing argon and oxygen with flow rates of 18 and 2 sccm, respectively. A ~5 nm thick LT-ZnO buffer layer was grown at 300 °C with working pressure of 1.0×10^{-2} Torr followed by an in situ annealing at 900 °C for 40 min. The purpose of growing a LT-ZnO buffer is to improve the surface morphology and to soften the strain resulting from the large lattice and thermal mismatches between ZnO and sapphire. The LT-ZnO buffer thus provides a better template for the subsequent ZnO growth. The growth of ZnO main layer was carried out at temperatures varying from 500 to 800 °C for 3 h with the pressure fixed at 5.0×10^{-3} Torr. The RF-power used for growing LT-ZnO buffer layer and ZnO films was 20 and 30 W, respectively. Finally, thermal annealing was performed at 1000 °C for 30 min.

X-ray measurements were conducted using a four-circle diffractometer at beamline BL13A of the National Synchrotron Radiation Research Center (NSRRC), Taiwan, with an incident wavelength of 1.027 Å. The cross-sectional TEM specimens with a thickness of about 90 nm were prepared by focused ion beam (FIB). TEM images were taken with a Philips TECNAI-20 field-emission gun type TEM. The polarized micro-Raman spectra with a He−Ne laser (632.8 nm) as the excitation source were recorded by a LabRam HR800 spectrometer (Jobin−Yvon, France).

■ RESULTS AND DISCUSSION

The XRD radial (θ−2θ) scans along the surface normal of the ZnO layers grown on m-plane sapphires with and without the LT-ZnO buffer layer are illustrated in scans a and b in Figure 1.

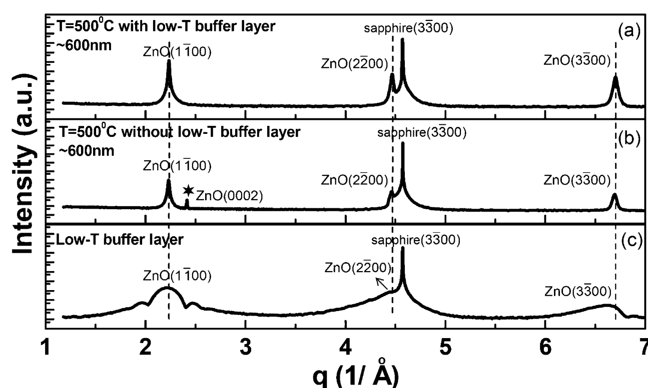

Figure 1. XRD radial scans along the surface normal of the ZnO layers grown on m-plane sapphire (a) with and (b) without the LT-ZnO buffer layer. The (★) in (b) marks the ZnO (0002) reflection from the c-plane oriented ZnO domains. (c) Radial scan of the sample of LT-ZnO layer alone.

The ZnO $(1\bar{1}00)$, $(2\bar{2}00)$, and $(3\bar{3}00)$ reflections were observed together with the sapphire $(3\bar{3}00)$ reflection, elucidating the crystalline orientation of $(1\bar{1}00)_{ZnO}$ ∥ $(1\bar{1}00)_{sapphire}$ along the surface normal. An additional weak peak located at ~2.41 Å^{-1} in Figure 1b is identified to be ZnO (0002) reflection, revealing the presence of c-plane oriented inclusions in the m-plane ZnO layer. The disappearance of the ZnO (0002) reflections in the sample buffered with a thin layer of LT-ZnO manifests that the buffer layer effectively eliminates the inclusions with undesirable c-plane orientation. Figure 1c illustrates the radial scan of the sample of a LT-ZnO layer alone. The ZnO $(n\bar{n}00)$ reflections are the dominant features, which elucidate the LT buffer layer has m-plane orientation already. The asymmetric line shape of the $(n\bar{n}00)$ reflections in Figure 1c, a signature of large strain gradient with the lattice stretched along the growth direction, reveals the significant strain relaxation occurring in the thin buffer layer. This relaxation leads to the smaller strain in the subsequently grown ZnO main layer as compared with the one without LT buffer layer, which is evidenced by the shift of the ZnO $(n\bar{n}00)$ reflections toward the larger scattering vector q and approaching the bulk peak position with the introduction of the LT buffer layer. The significant decrease in the peak width of the X-ray θ-rocking curve, not shown here, also reveals the improvement in crystalline quality of the ZnO films with the LT buffer layer.

In Figure 1c, we also note the pronounced interference fringes, known as the thickness fringes, near the ZnO$(1\bar{1}00)$ Bragg peak of the buffer layer. The presence of the thickness fringe is an indication of sharp interface and good crystalline structure. From the fringe period, Δq = 0.125 Å^{-1}, we determined the thickness of the LT-ZnO buffer layer to be ~5 nm. Furthermore, the LT-ZnO buffer is epitaxially grown on m-plane sapphire as demonstrated by the XRD azimuthal cone scans (ϕ-scans) across the off-specular reflections. The left and right panels of Figure 2 illustrate, respectively, the azimuthal

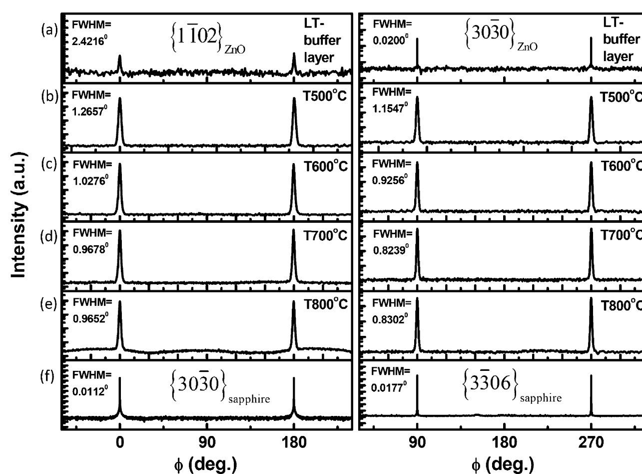

Figure 2. XRD azimuthal ϕ-scans across (a) ZnO $\{10\bar{1}2\}$ and sapphire $\{30\bar{3}0\}$ and (b) ZnO $\{30\bar{3}0\}$ and sapphire $\{3\bar{3}06\}$ reflections. The growth temperature of the ZnO films varies from 500 to 800 °C.

scans across the ZnO $\{1\bar{1}02\}$ and $\{30\bar{3}0\}$ reflections of the LT buffer layer (see the row labeled with a), and the ZnO samples grown at various temperatures shown in rows b−e. The two 180° separated peaks verify the expected 2-fold symmetry against the surface normal. By comparing the angular positions of these peaks relative to the sapphire $\{30\bar{3}0\}$ and $\{3\bar{3}06\}$ reflections, illustrated in row f, we concluded that the in-plane epitaxial relation of this heteroepitaxial system follows $(11\bar{2}0)_{ZnO}$ ∥ $(0006)_{sapphire}$ and $(0002)_{ZnO}$ ∥$(11\bar{2}0)_{sapphire}$, and the LT-ZnO buffer layer is fully epitaxial already. The LT-ZnO epitaxial buffer layer provides not only a significantly less mismatched template but also a flatter surface for the subsequent growth of the ZnO main layer. Surface morphology measurements by AFM confirm the reduction of surface root-mean-square roughness from 5.0 Å of m-sapphire surface to 1.7 Å of LT-ZnO surface that also contributes to the crystalline quality improvement in the ZnO main layer.

Growth temperature is another factor affecting the structural perfection of the ZnO films. Twist and tilt angles are two parameters commonly adopted to examine the structural quality of an epitaxial film. The twist angle can be represented by the azimuthal peak width of off normal reflections. The small

value of full width at half-maximum (fwhm), less than 1°, of the azimuthal scans, shown in Figure 2b–e, manifests the good crystalline quality of m-plane ZnO epi-layers. The monotonic decrease in the peak width with increasing growth temperature indicates the improving crystalline structure at higher growth temperature. Similar trend was also observed in the tilt angle, which can be represented by the θ-rocking curve of the specular reflections. The left and right panels of Figure 3 present the X-ray θ-rocking curves (XRCs) of the ZnO $(3\bar{3}00)$ reflection of the samples grown at various temperatures with the incident X-ray beams impinging perpendicular and parallel to the *c*-axis of the m-plane ZnO films, respectively. The line width monotonically decreases with increasing growth temperature regardless of the incident direction implying the progressive improvement of the film structure with elevated temperature. Even though the sample grown at 800 °C has slightly narrower peak width than the one grown at 700 °C, additional broad weak features were observed in the background of the azimuthal scan shown in Figure 2e, implying the formation of other structure. Thus, growth temperature of ~700 °C yields the m-plane ZnO film with optimal structure.

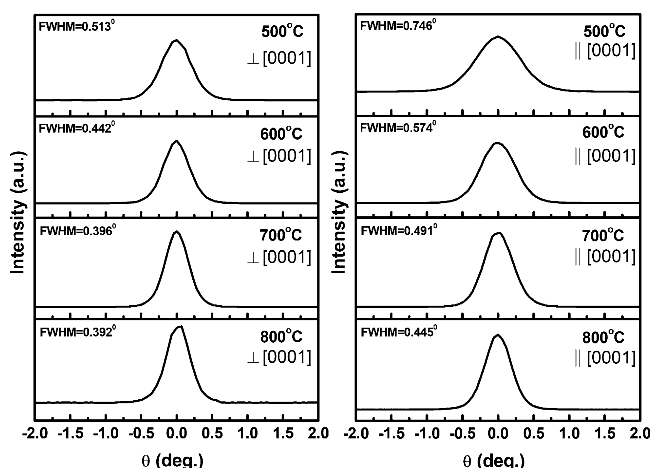

Figure 3. X-ray rocking curves of the ZnO $(3\bar{3}00)$ reflection with the incident X-ray (a) perpendicular and (b) parallel to the *c*-axis of the m-plane ZnO films.

It is noteworthy that the specular reflections exhibit anisotropic line width with respect to the X-ray incident direction. The peak widths measured with X-ray perpendicular to the *c*-axis, left panel of Figure 3, are systematically narrower than that with X-ray along the *c*-axis, right panel of Figure 3. As a contrast, the rocking curves of a m-plane ZnO wafer measured along the two orthogonal directions exhibit the same width (~0.03°), which rules out the intrinsic line width difference originated from the crystal structure. These results indicate that the m-plane ZnO epi-layers are crystallographically more perfect along the $[11\bar{2}0]$ direction than the [0001] direction. Similar azimuthal anisotropy has also been observed in m-plane GaN grown on m-plane sapphire,[16] where the anisotropic broadening of the XRCs was attributed to the striped surface morphology.[17] However, no stripelike features were found in the AFM surface images of our samples. We believe that the observed azimuthal dependent line width is a reflection of the asymmetric nature of the microstructure, which will be discussed below.

In order to investigate the microstructure of the samples, cross sectional TEM images were recorded near the ZnO/sapphire interface along two orthogonal directions. Shown in images a and b in Figure 4 are the micrographs of the sample grown at 700 °C taken along the ZnO [0001] and $[11\bar{2}0]$ zone axes, respectively. The corresponding selected area electron diffraction (SAED) patterns are also shown in images c and d in Figure 4, which confirm the epitaxial relationship determined by XRD and the absence of domains with other orientation. Both micrographs illustrate the atomic sharp ZnO/sapphire interface but the interface between the LT-ZnO buffer layer and the ZnO main layer, as noted by the dashed lines, can hardly be recognized. Much more structural defects are identified in Figure 4b distributed along the [0001] direction; this accounts for the larger peak width of the θ-rocking curves measured with X-ray incident parallel to the ZnO *c*-axis.

According to the determined epitaxial relationship, $(11\bar{2}0)_{ZnO} \parallel (0006)_{sapphire}$ and $(0002)_{ZnO} \parallel (11\bar{2}0)_{sapphire}$, the lattice mismatch $(a_f - a_s)/a_s$ with a_f and a_s denoting respectively the lattice constant of the film and substrate, is −75.0% along the ZnO $[11\bar{2}0]$ and 9.5% along the ZnO [0001] direction. The m-ZnO films thus experience a strong anisotropic deformation due to different lattice and thermal mismatch between ZnO and the underlying substrate along two orthogonal lateral directions. Figure 4e illustrates the local magnification of the micrograph taken near the ZnO/sapphire interface with the ZnO [0001] zone axis. Consistent with the results reported by Chauveau et al.[9] that domain matching epitaxy (DME)[18] is achieved along the ZnO $[11\bar{2}0]$ direction with domains made of four ZnO $(11\bar{2}0)$ planes matching domains consisting of three sapphire (0006) planes. Periodically arranged white spots were observed near the ZnO/sapphire interface along the ZnO $[11\bar{2}0]$ direction. The average spacing ~6.7 Å between the spots is in good agreement with the expected domain size, four times the ZnO $(11\bar{2}0)$ interplanar distance, that reflects the variation of local strain field caused by the extra half plane inserted in each ZnO domain. The huge lattice mismatch is thus accommodated by the misfit dislocations and yields an effective lattice mismatch of −0.1%, which explains the observed good crystalline quality along the direction perpendicular to the *c*-axis.

Along the other in-plane direction, the ZnO [0001] direction, the interface structure is not as order as that along the $[11\bar{2}0]$ direction and conforms to neither DME nor lattice matching epitaxy (LME). Lines of defects running along the growth direction, as marked by the arrows in Figure 4b, distribute irregularly in the ZnO layer, which are identified as the basal plane stacking faults. The HR-TEM image of a BSF, as indicated by the variation of stacking sequence, is shown in Figure 4f and the BSF density is about 4×10^5 cm^{-1}. The adverse effects of the BSFs are not only causing in-plane carrier separation and junction leakage current[19] but also reducing internal quantum efficiency in ZnO LED devices. Therefore, reducing the BSFs density is essential to improve the nonpolar device performance.

The lateral anisotropic characteristics of the m-ZnO layers are also reflected in their polarized Raman spectra. Curves a and b in Figure 5 depict the Raman spectra of the 700 °C sample taken in two distinct backscattering geometries, $X(ZZ)\bar{X}$ and $X(YY)\bar{X}$ with the laser polarization $\hat{E}$ aligned with the *Z* and *Y* axes, respectively. A schematic of the scattering geometry is depicted in the up right corner in Figure 5, where the *X*, *Y*, and *Z* axes are, respectively, along the ZnO

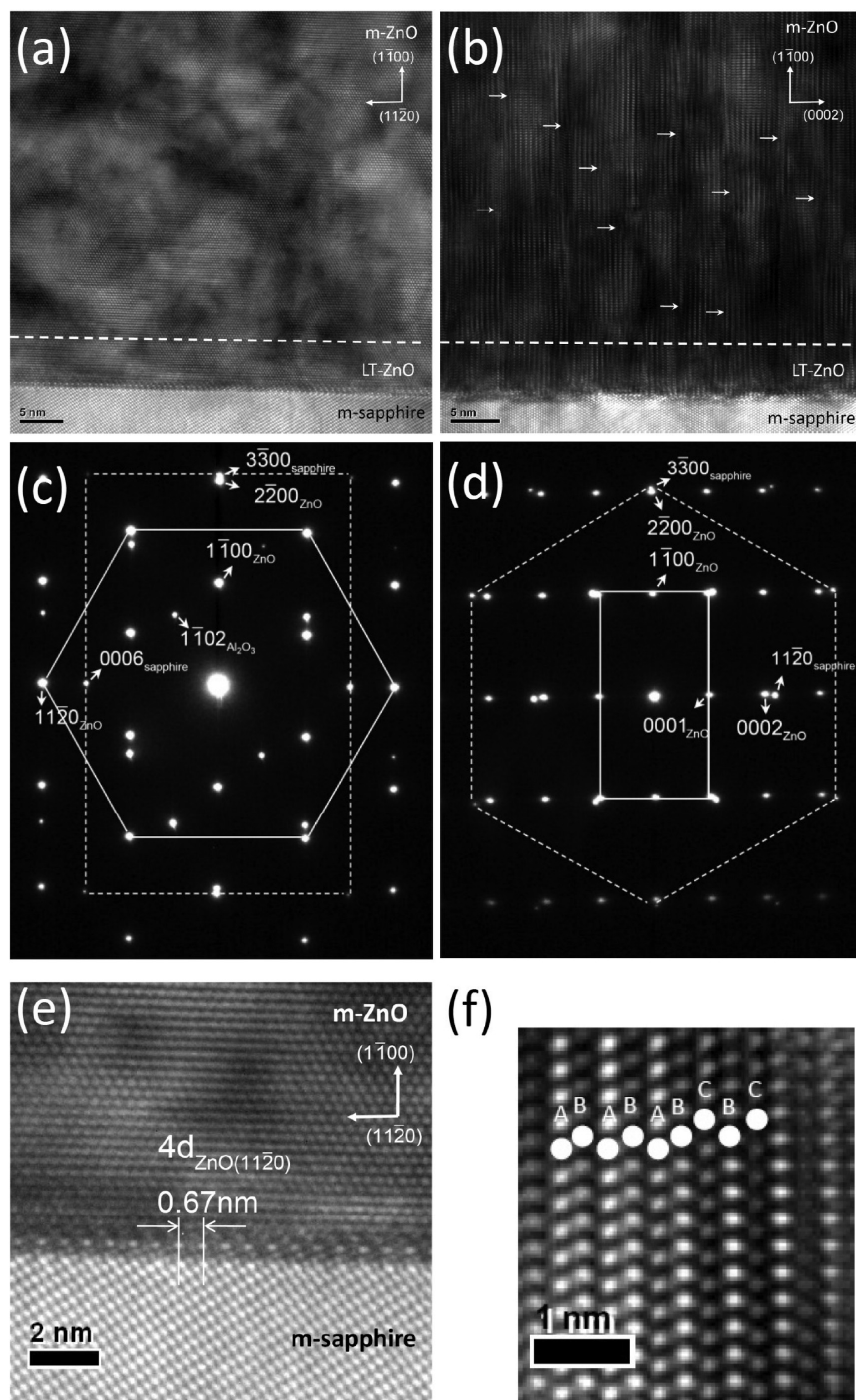

Figure 4. (a, b) Cross-sectional HR-TEM images taken with the zone axis along the $[0002]_{ZnO}$ and $[11\bar{2}0]_{ZnO}$, respectively. (c, d) SAED patterns recorded at the ZnO/sapphire interface with the $[0002]_{ZnO}$ and $[11\bar{2}0]_{ZnO}$ zone axes. (e) Magnified image near ZnO/sapphire interface with the $[0002]_{ZnO}$ zone axis, in which the periodic strain contrast is clearly observed. (f) Atomic image near a basal plane stacking fault.

surface normal, $[11\bar{2}0]$, and *c*-axis. The polarization angle ω denotes the rotation angle of $\hat{E}$ in the $Y-Z$ plane away from the ZnO $[11\bar{2}0]$ axis. The intense peak at 417.0 cm^{-1} comes from the sapphire substrate (A_{1g} phonon mode) as evidenced by sapphire PL spectrum shown by curve c. The Raman peaks at 377.7 and 436.4 cm^{-1} are attributed to the ZnO $A_1(TO)$, and E_2(high) phonon modes, respectively. The ZnO $E_1(TO)$ mode located at 410.3 cm^{-1} is barely seen in the base of the intense sapphire A_{1g} mode in the $X(YZ)\bar{X}$ and $X(ZY)\bar{X}$ cross-polarization geometries (not shown). Wurtzite ZnO belongs to the space group C_{6v} and according to the Raman selection rules,[20] the E_2(high) mode is forbidden as the laser polarization

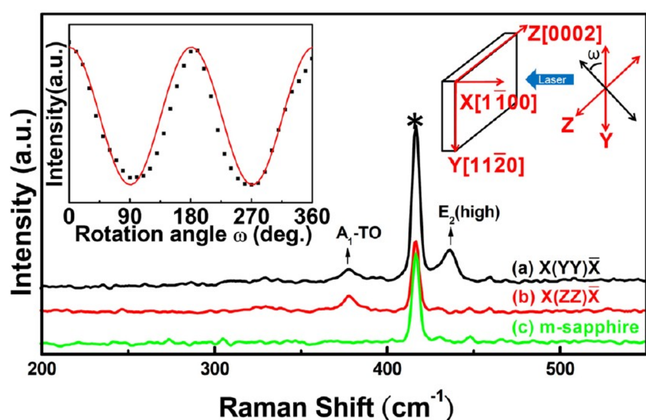

Figure 5. Polarized micro-Raman scattering spectra of the m-ZnO/sapphire sample under $X(YY)\bar{X}$ (top) and $X(ZZ)\bar{X}$ (middle) parallel polarization geometries. The spectrum of a sapphire substrate is also shown in the bottom for comparison. The schematics of the scattering geometry and the definition of the rotation angle are depicted in the upper right corner. The inset shows the intensity variation of the ZnO E_2(high) mode as a function of the rotation angle ω. The filled squares depict the experimental data; the fitting results using a $\cos^2(\omega)$ function is displayed by the solid curve.

$\hat{E}$ is parallel to the ZnO *c*-axis. The emergence/disappearance of the peak at 436.4 cm^{-1} in the $X(ZZ\bar{X})$/ $X(YY)\bar{X}$ geometry agrees with the expected polarization dependence of the E_2(high) mode. Moreover, the intensity of the E_2(high) mode exhibits an oscillatory variation with 2-fold symmetry as a function of the rotation angle ω of the polarizer in front of the detector as depicted by the filled squares in the inset. The angular dependence of the E_2(high) intensity can be reasonably well-fitted by a $\cos^2(\omega)$ function, as depicted by the solid curve in the inset. The peaks in the measured spectra all exhibit the same polarization dependence as bulk ZnO implying the obtained film retains the hexagonal symmetry. This observation also agrees with the XRD results, which show the strain along the $[10\bar{1}0]$ and $[11\bar{2}0]$ directions of the annealed samples are very similar (both ∼0.2%). The red shift of the E_2(high) mode as compared with the unstressed ZnO is attributed to the residual tensile stress in the films. In contrast, the m-plane ZnO grown on m-plane sapphire by PLD exhibits a different strain state. The lattice is stressed tensily (∼0.6%) along the $[10\bar{1}0]$ direction and compressively (approximately −0.2%) along the $[11\bar{2}0]$ direction, resulting in the transformation to an orthogonal lattice. The more relaxed lattice structure of the ZnO grown by RF sputtering deposition may be attributed to the smaller grain size as compared with that grown by PLD as indicated by the XRD and TEM results.

CONCLUSIONS

We demonstrated that high-quality, single-domain m-plane ZnO epi-films can be grown on m-plane sapphire by applying RF-magnetron sputtering deposition. The introduction of a nanometer-thick LT-ZnO buffer layer effectively removes the undesirable extra orientations and improves the structural perfection of the ZnO films. The structural quality of the ZnO layers so obtained is comparable or even superior to that of the ZnO layers grown by other methods, such as plasma-assisted molecular beam epitaxy[17] and atomic layer deposition[10] as judged from the line widths of XRD peaks. Similar to the nonpolar ZnO films grown by other methods, BSFs are still the major structural defects in these ZnO layers. Both XRD and polarized Raman scattering results demonstrate that the obtained m-ZnO films are of single orientation and retain the hexagonal symmetry. Furthermore, no obvious variation in both structural and optical characteristics was detected at different portion of the sample, indicating that the epitaxy is maintained laterally with the same quality along the whole sample size, an important feature for a practical point of view.

AUTHOR INFORMATION

Corresponding Author

*E-mail: chsu@nsrrc.org.tw (C.-H.H.); wfhsieh@mail.nctu.edu.tw (W.F.H.). Tel: 886-3-578-0281 x7118 (C.-H.H.); 886-3-571-2121 x56316 (W.F.H.). Fax: 886-3-578-3813 (C.-H.H.); 886-3-571-6631 (W.F.H.).

Notes

The authors declare no competing financial interest.

ACKNOWLEDGMENTS

The National Science Council (NSC) of Taiwan supported this work under Contracts NSC-99-2112-M-006-017-MY3 and NSC-100-2112-M-213-003-MY3.

REFERENCES

(1) Bernardini, F.; Fiorentini, V.; Vanderbilt, D. *Phys. Rev. B* **1997**, *56*, R10024.
(2) Gil, B.; Lefebvre, P.; Bretagnon, T.; Guillet, T.; Sans, J. A.; Taliercio, T.; Morhain, C. *Phys. Rev. B* **2006**, *74*, 153302.
(3) Iwata, K.; Asahi, H.; Asami, K.; Kuroiwa, R.; Gonda, S. *Jpn J. Appl. Phys.* **1997**, *36*, L661.
(4) Lee, J. W.; Kim, J.-H.; Han, S. K.; Hong, S.-K.; Lee, J. Y.; Hong, S. I.; Yao, T. *J. Cryst. Growth* **2010**, *312*, 238.
(5) Baker, T. J.; Haskell, B. A.; Wu, F.; Speck, J. S.; Nakamura, S. *Jpn J. Appl. Phys.* **2006**, *45*, L154.
(6) Lahourcade, L.; Bellet-Amalric, E.; Monroy, E.; Abouzaid, M.; Ruterana, P. *Appl. Phys. Lett.* **2007**, *90*, 131909.
(7) Onuma, T.; Amaike, H.; Kubota, M.; Okamoto, K.; Ohta, H.; Ichihara, J.; Takasu, H; Chichibu, S. F. *Appl. Phys. Lett.* **2007**, *91*, 181903.
(8) Kuo, C. C.; Lin, B. H.; Yang, Song; Liu, W. R.; Hsieh, W. F.; Hsu, C.-H. *Appl. Phys. Lett.* **2012**, *101*, 011901.
(9) Chauveau, J.-M.; Vennéguès, P.; Laügt, M.; Deparis, C.; Zuniga-Perez, J.; Morhain, C. *J. Appl. Phys.* **2008**, *104*, 073535.
(10) Ku, C.-S.; Lee, H.-Y.; Huang, J.-M.; Lin, C.-M. *Cryst. Growth Des.* **2010**, *10*, 1460.
(11) Chou, M. M. C.; Chang, L.; Hang, D.-R.; Chen, C.; Chang, D.-S.; Li, C.-A. *Cryst. Growth Des.* **2009**, *9*, 2073.
(12) Wang, W.-L.; Ho, Y.-T.; Chiu, K.-A.; Peng, Chun-Yen; Chang, L. *J. Cryst. Growth* **2010**, *312*, 1179.
(13) Atuchin, V. V.; Galashov, E. N.; Kozhukhov, A. S.; Pokrovsky, L. D.; Shlegel, V. N. *J. Cryst. Growth* **2011**, *318*, 1147.
(14) Lin, H.; Zhou, S.; Huang, T.; Teng, H.; Liu, X.; Gu, S.; Zhu, S.; Xie, Z.; Han, P.; Zhang, R. *J. Alloys Compd.* **2009**, *467*, L8.
(15) Cagin, E.; Yang, J.; Wang, W.; Phillips, J. D.; Hong, S. K.; Lee, J. W.; Lee, J. Y. *Appl. Phys. Lett.* **2008**, *92*, 233505.
(16) Armitage, R.; Hirayama, H. *Appl. Phys. Lett.* **2008**, *92*, 092121.
(17) Kim, J.-H.; Han, S. K.; Hong, S. I.; Hong, S.-K.; Lee, J. W.; Lee, J. Y.; Song, J.-H.; Park, J. S.; Yao, T. *J. Vac. Sci. Technol. B* **2009**, *27*, 1625.
(18) Narayan, J.; Larson, B. C. *J. Appl. Phys.* **2003**, *93*, 278.
(19) Chakraborty, A.; Haskell, B. A.; Keller, S.; Speck, J. S.; Denbaars, S. P.; Nakamura, S.; Mishra, U. K. *Jpn J. Appl. Phys.* **2005**, *44*, L173.
(20) Damen, T. C.; Porto, S. P. S.; Tell, B. *Phys. Rev.* **1966**, *142*, 570.